Fast live cell imaging at nanometer scale using annihilating filter based low rank Hankel matrix approach

Junhong Min[a] and Lina Carlini[c] and Michael Unser[b] and Suliana Manley[c] and Jong Chul Ye[a]

[a]Department of Bio and Brain Engineering, korean advanced institute of science and technology, Daejeon, Republic of Korea;
[b]Institute of the Physics of Microengineering, École polytechnique fédérale de Lausanne, Switzerland;
[c]Institute of the Physics of Biological Systems,École polytechnique Fédérale de Lausanne, Switzerland

ABSTRACT

Localization microscopy such as STORM/PALM can achieve a nanometer scale spatial resolution by iteratively localizing fluorescence molecules. It was shown that imaging of densely activated molecules can accelerate temporal resolution which was considered as major limitation of localization microscopy. However, this higher density imaging needs to incorporate advanced localization algorithms to deal with overlapping point spread functions (PSFs). In order to address this technical challenges, previously we developed a localization algorithm called FALCON[1,2] using a quasi-continuous localization model with sparsity prior on image space. It was demonstrated in both 2D/3D live cell imaging. However, it has several disadvantages to be further improved. Here, we proposed a new localization algorithm using annihilating filter-based low rank Hankel structured matrix approach (ALOHA). According to ALOHA principle, sparsity in image domain implies the existence of rank-deficient Hankel structured matrix in Fourier space. Thanks to this fundamental duality, our new algorithm can perform data-adaptive PSF estimation and deconvolution of Fourier spectrum, followed by truly grid-free localization using spectral estimation technique. Furthermore, all these optimizations are conducted on Fourier space only. We validated the performance of the new method with numerical experiments and live cell imaging experiment. The results confirmed that it has the higher localization performances in both experiments in terms of accuracy and detection rate.

Keywords: Annihilating filter, Low-rank, Hankel matrix, Matrix pencil, Localization, Microscopy, Super-resolution, High-density

1. INTRODUCTION

Localization microscopy such as STORM/PALM[3–5] can achieve super-resolution imaging over diffraction-limit using a field optical system. This resolution breakthrough attributes to the facts: 1. localization precision of a single molecule is not diffraction-limited, 2. fluorescence emission events of molecules can be controlled to spread out in time by harnessing non-linear photo-physics of fluorescent molecules. Specifically, fluorescence molecules are sparsely activated at each time frame, separating molecules spatio-temporally. Then, the activated molecules are localized, which can be done up to nanometer scale. After repeating this process until enough molecules are localized, a super-resolution(sr) image is constructed in the form of a histogram or a Gaussian-rendered image. However, this conventional low-density acquisition generally leads to a long acquisition time for a single sr image in order to collect numerous locations of molecules. Actually, this can be seen as trade-off between the spatial resolution and the temporal resolution. Thus, the conventional localization microscopy has limitations on live cell imaging due to the slow temporal resolution.

To deal with the issue of slow temporal resolution, a high-density imaging can be used. Literally, it acquires raw data at a higher molecular density, so that more molecules can be localized, accelerating a temporal resolution.

Further author information: (Send correspondence to Jong Chul Ye): E-mail: jong.ye@kaist.ac.kr
This work was supported by NRF-2015M3A9A7029734 and NRF-2014R1A2A1A11052491

Wavelets and Sparsity XVI, edited by Manos Papadakis, Vivek K. Goyal, Dimitri Van De Ville,
Proc. of SPIE Vol. 9597, 95970V · © 2015 SPIE · CCC code: 0277-786X/15/$18
doi: 10.1117/12.2187393

However, the localization task is not trivial because a raw image frame contains many overlapping point spread functions (PSFs). Several localization methods[1,2,6–8] have been proposed to resolve the overlapping PSFs. For example, multi-emitter fitting methods[6,7] fit multiple PSFs to the data in a greedy manner. In other approach,[8] localizations are performed by image deconvolution of the raw data. Specifically, it imposes sparsity-priors such as l_1 norm on a sub-pixel discrete grid to recover a sparse sub-pixel image. This approach has been demonstrated to recover more localizations than the greedy approach. However, since it has intrinsic localization artifacts due to its discrete formulation, the deconvolution should be performed in a very fine scale sub-pixels, which leads to huge computational cost. To overcome this disadvantage, we introduced a localization algorithm called FALCON[1,2] using quasi-continuous localization model. Specifically, it combines a sparse deconvolution with Taylor approximation of PSF to assimilate a PSF, shifted from the grid point. This off-grid technique can reduce not only localization artifacts but also computational cost significantly. FALCON was also demonstrated in 3D localization[2] with a modified imaging system, combined with astigmatic and biplane imaging.

Although our previous works had addressed many localization issues in the high-density imaging, there is still room for improvement. First, the image deconvolution based approaches[1,7,8] commonly require prior knowledge of PSF that is usually estimated from an additional low-density training dataset. To take the training dataset is usually counted as additional burden on experiments. More importantly, a predefined single PSF model cannot be fully fitted to the data because PSF generally varies spatio-temporally during acquisition of data in live cell imaging. Thus, PSF should be locally estimated from the raw data frame. Furthermore, our previous work on quasi-continuous localization model using off-grid technique does not fully assimilate real continuous space. Moreover, it still needs a coarse sub-pixel grid to minimize Taylor approximation errors of off-grid PSF. In addition, this first-order Taylor approximation is affected by imperfection of pre-estimated PSF.

Here, we proposed a new localization algorithm using annihilating filter-based low rank Hankel structured matrix approach (ALOHA) which was recently proposed by our group for MR imaging[9] and image inpainting.[10] According to these works,[9,10] sparsity prior in image space can be interpreted as existence of a rank-deficient Hankel structured matrix in Fourier space. Based on this fundamental duality, our new algorithm fully utilizes this low-rankness, allowing data-adaptive and grid-free localizations in Fourier domain. Specifically, the algorithm is locally applied to several image patches. First, PSF is independently estimated from each patch by a parametric optimization, and then, entire Fourier spectrum of each patch is recovered by using Fourier-based non-blind deconvolution. Finally, a matrix pencil based harmonic retrieval algorithm called ACMP is applied to the spectrum for the truly grid-free localizations. All these optimization steps are processed on Fourier space only. We validated the performance of the new method with numerical experiments and live imaging of mitochondria experiment. The results confirmed that it is more robust to the high-density imaging, showing higher scores of performance measures in terms of accuracy and detection rate.

2. BACKGROUND

2.1 Principle of Annihilating Filter-based Low rank Hankel Structured Matrix Approach

In general, we can describe a K sparse signal $f(\boldsymbol{\rho}) \in \mathbb{R}^2$ as follows,

$$f(\boldsymbol{\rho}) = \sum_{k=1}^{K} c_k \delta(\boldsymbol{\rho} - \boldsymbol{\rho}_k), \tag{1}$$

where $\boldsymbol{\rho}_k$ is the position of the k-th source and c_k is its signal intensity. It is easy to show that there always exists an annihilating function $a(\boldsymbol{\rho})$ which has a distinct support set from f:.

$$a(\boldsymbol{\rho}) f(\boldsymbol{\rho}) = 0 \ . \tag{2}$$

Thus, it directly implies that the corresponding annihilating filter $\hat{a}(\boldsymbol{\omega}) := \mathcal{F}\{a(\boldsymbol{\rho})\}, \boldsymbol{\omega} = (\boldsymbol{\omega}_x, \boldsymbol{\omega}_y)$ also exists in Fourier domain:

$$\hat{a}(\boldsymbol{\omega}) * \hat{f}(\boldsymbol{\omega}) = 0 \ . \tag{3}$$

For discrete signal case, this convolution Eq. (3) can be rewritten as a matrix-vector form:

$$\mathscr{H}\{\hat{\mathbf{F}}\} \text{VEC}(\hat{\mathbf{A}})^{\vee} = \mathbf{0}, \tag{4}$$

where $\hat{\mathbf{F}} = [\mathbf{f}_1, \cdots, \mathbf{f}_N] \in \mathbb{R}^{M\times N}$ and $\hat{\mathbf{A}} = [\mathbf{a}_{-n}, \cdots, \mathbf{a}_n] \in \mathbb{R}^{(2m+1)\times(2n+1)}$ are the matrices containing Fourier coefficients, and the annihilating filter coefficients, respectively. $\mathscr{H}\{\hat{\mathbf{F}}\}$ is the block Hankel matrix constructed from $\hat{\mathbf{F}}$, $\text{VEC}(\hat{\mathbf{A}})$ is the vectorized annihilating filter and $\vee$ is order reversal operator. This the block Hankel structured matrix $\mathscr{H}\{\hat{\mathbf{F}}\}$ is simply generated by partitioning and stacking operations:

$$\mathscr{H}\{\mathbf{F}\} = \begin{bmatrix} \mathcal{H}\{\mathbf{f}_1\} & \mathcal{H}\{\mathbf{f}_2\} & \cdots & \mathcal{H}\{\mathbf{f}_{2n+1}\} \\ \mathcal{H}\{\mathbf{f}_2\} & \mathcal{H}\{\mathbf{f}_3\} & \cdots & \mathcal{H}\{\mathbf{f}_{2n+2}\} \\ \vdots & \vdots & \ddots & \vdots \\ \mathcal{H}\{\mathbf{f}_{N-2n}\} & \mathcal{H}\{\mathbf{f}_{N-2n+1}\} & \cdots & \mathcal{H}\{\mathbf{f}_N\} \end{bmatrix} \in \mathbb{R}^{(M-2m)(N-2n)\times(2m+1)(2n+1)} . \tag{5}$$

where $\mathcal{H}\{\mathbf{f}_i\}$ is defined by

$$\mathcal{H}\{\mathbf{f}_i\} = \begin{bmatrix} \mathbf{f}_i(1) & \mathbf{f}_i(2) & \cdots & \mathbf{f}_i(2m+1) \\ \mathbf{f}_i(2) & \mathbf{f}_i(3) & \cdots & \mathbf{f}_i(2m+2) \\ \vdots & \vdots & \ddots & \vdots \\ \mathbf{f}_i(M-2m) & \mathbf{f}_i(M-2m+1) & \cdots & \mathbf{f}_i(M) \end{bmatrix} \in \mathbb{R}^{(M-2m)\times(2m+1)} .$$

Importantly, it is known[9,10] that rank of $\mathscr{H}\{\hat{\mathbf{F}}\}$ is given by

$$\text{rank}\mathscr{H}\{\hat{\mathbf{F}}\} = \min\{K, M-2m+1\} \tag{6}$$

Thus, the sparse image can be directly inferred to as existence of a rank-deficient Hankel structured matrix, which is low-ranked. This fundamental duality between the sparsity and low-rankness can be utilized for the reconstruction of any continuous sparse signal, not limited to discrete domain.

2.2 Imaging Model of Localization Microscopy

In localization microscopy, K active fluorescent molecules at a given time instant can be also described as a collection of ideal point sources like Eq. 1. Here, measurements; camera images, are obtained through a conventional wide-field microscopy which is a band-limited system. Thus, the camera image is represented as the following convolution form with additive noises:

$$g[\boldsymbol{\rho}] \sim \sum_{k=1}^{K} c_k\, h(\boldsymbol{\rho} - \mathbf{x}_k) + \mathbf{n}[\boldsymbol{\rho}] \tag{7}$$

where h is the PSF of the microscope and $\mathbf{n}$ represents random noise perturbations including background autofluorescence and camera noises. Accordingly, it can be written as

$$\hat{G}[\boldsymbol{\omega}] = \hat{H}[\boldsymbol{\omega}]\hat{F}[\boldsymbol{\omega}] + \hat{N}[\boldsymbol{\omega}], \tag{8}$$

where $\hat{G}[\boldsymbol{\omega}]$,$\hat{H}[\boldsymbol{\omega}]$ and $\hat{F}[\boldsymbol{\omega}]$ are corresponding discrete Fourier coefficients of g, h and f, respectively. Because the fluorescent probes can be regardless as infinitesimal points, in noiseless case, we can well approximate $\hat{F}$ as sum of K frequency harmonics:

$$\hat{F}[\boldsymbol{\omega}] = \frac{\hat{G}[\boldsymbol{\omega}]}{\hat{H}[\boldsymbol{\omega}]} \simeq \sum_{k=1}^{K} c_k e^{-j2\pi\boldsymbol{\omega}_k}, \quad \boldsymbol{\omega}_k = \left(\frac{x_k}{M}, \frac{y_k}{N}\right) \in \Omega, \tag{9}$$

where Ω is a passband of the PSF $\hat{H}[\boldsymbol{\omega}]$ whose values are non-zero. This implies that localizations of point sources can be considered as a conventional harmonics retrieval problem.[11,12]

3. PROPOSED LOCALIZATION ALGORITHM

In this section, we explain our new localization algorithm based on ALOHA principle. The algorithm starts to divide a raw image frame into several patches as shown in Fig.1. This patch-based approach allows more data-adaptive localization. Specifically, the algorithm consists of following three steps: 1. data-adaptive PSF estimation, 2. deconvolution of Fourier spectrum, 3. grid-free localization using a matrix-pencil based harmonic retrieval algorithm. The details of each step are illustrated in the following sections.

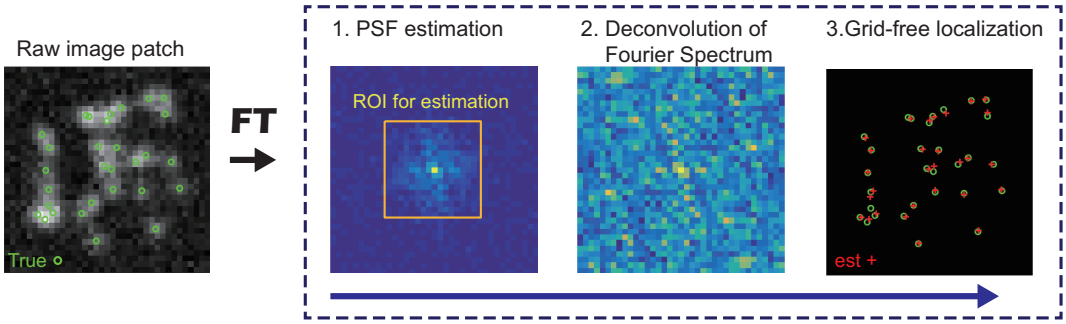

Figure 1. Schematic illustration for the proposed method.

3.1 Parametric PSF Estimation

In most of the localization microscopy, PSF is modelled as a 2 dimensional symmetric Gaussian function $\mathbf{h}_\sigma(\boldsymbol{\rho}) = \frac{1}{2\pi\sigma^2} e^{\left(-\frac{\rho^2}{2\sigma^2}\right)}$. In this assumption, PSF estimation problem is nothing but a single parameter estimation in terms of σ. Furthermore, according to ALOHA principle, we already know that a sparse signal can be transformed as a low-rank Hankel matrix of its Fourier spectrum $\hat{F}[\boldsymbol{\omega}]$. Accordingly, a Hankel matrix $\mathscr{H}\{\frac{\hat{G}[\boldsymbol{\omega}]}{\hat{H}_\sigma[\boldsymbol{\omega}]}\}$ has the lowest rank if the $\hat{H}_\sigma[\boldsymbol{\omega}]$ is equal to the true PSF spectrum $\hat{H}[\boldsymbol{\omega}]$. Therefore, PSF can be estimated by finding the parameter σ_* to make the minimum rank of $\mathscr{H}\{\frac{\hat{G}[\boldsymbol{\omega}]}{\hat{H}_\sigma[\boldsymbol{\omega}]}\}$. Specifically, the estimation is done by minimizing Schatten-p norm of the Hankel matrix as follows:

$$\sigma_* = \min_{\sigma} \left\| (\mathscr{H}\{\frac{\hat{G}[\boldsymbol{\omega}]}{\hat{H}_\sigma[\boldsymbol{\omega},]}\} \right\|_p, \quad \boldsymbol{\omega} \in \Omega, \quad 0 < p \leq 1. \tag{10}$$

This single-variable non-linear optimization can be performed very quickly by golden section search. More specifically, we used a built-in MATLAB function "**fminbnd**".

3.2 Deconvolution of Fourier spectrum

After PSF estimation, it then recovers the Fourier spectrum $\hat{F}$ from the band-limited $\hat{G}$ by using non-blind deconvolution. Based on the duality of sparse signal, the spectrum can be retrieved by minimizing a penalized least-squares with a low-rank penalty of Hankel matrix $\mathscr{H}\{\hat{F}\}$. Moreover, in Fourier domain, the cost function can be simplified as follows:

$$\begin{aligned} \min_{\hat{F}} \quad & \|\hat{G} - \hat{H} \odot \hat{F}\|_F^2 + \lambda \|\mathscr{H}\{\hat{F}\}\|_*, \\ & s.t. \quad f \in \mathbb{R} \end{aligned} \tag{11}$$

This nuclear norm minimization problem can be efficiently tackled by using a variable-splitting method such as ADMM.[13] By using ADMM, the Eq. 11 is rewritten as an alternating minimization form:

$$\begin{aligned} \min_{\hat{F},U,D} \quad & \|\hat{G} - \hat{H} \odot \hat{F}\|_F^2 + \lambda \|U\|_* + \mu \|U - \mathscr{H}\{\hat{F}\} + D\|_F^2, \\ & s.t. \quad f \in \mathbb{R} \end{aligned} \tag{12}$$

In this form, the data fidelity term and the penalty term can be handled separately. As a result, the full Fourier spectrum $\hat{F}$ is recovered by updating these three variables alternatively. The update rules are summarized in the following box.

Deconvolution of Fourier spectrum

$$\hat{F}_{i+1}[\boldsymbol{\omega}] = \mathcal{P}\Big(\frac{\hat{H}^*[\boldsymbol{\omega}]\hat{G}[\boldsymbol{\omega}] + \mu\mathscr{H}^*\{U_i + D_i\}[\boldsymbol{\omega}]}{|\hat{H}[\boldsymbol{\omega}]|^2 + \mu W_{\mathscr{H}}[\boldsymbol{\omega}]}\Big), \quad (13)$$

$$\hat{U}_{i+1} = \mathcal{SVD}_{th}\left(\mathscr{H}\{\hat{F}_{i+1}\} - D_i, \frac{\lambda}{\mu}\right), \quad (14)$$

$$D_{i+1} = D_i + U_{i+1} - \mathscr{H}\{\hat{F}_{i+1}\} \quad (15)$$

Here, $\mathcal{P}$ is a Hermitian-symmetry projection operator to impose "real" signal constraint, $\mathcal{SVD}_{th}$ is an operator of soft singular value thresholding, and the matrix $W_{\mathscr{H}}$ is defined as

$$W_{\mathscr{H}}^{M\times N} = \mathscr{H}^*\{\mathscr{H}\{\mathbf{1}^{M\times N}\}\}$$

where $\mathbf{1}$ is a matrix whose entries are all one. Since all updates are performed on Fourier-domain, the spectrum $\hat{F}$ is efficiently updated in point-wise manner. In fact, the most computation complexity is attributed to updating U because of high-computational cost of the singular value decomposition. However, since the rank of K is usually sparse, this computational complexity can be quite reduced by using matrix factorization techniques[10] or randomized SVD methods.[14]

3.3 Grid-free localization using Matrix Pencil method

After deconvolution of Fourier spectrum, finally locations of sources are extracted from the spectrum. As we mentioned above, this process is nothing but the conventional harmonic retrieval problem. Here, we used a matrix pencil based algorithm called ACMP (algebraically coupled matrix pencils). A basic ACMP algorithm will be briefly explained.

Under assumption that harmonic components in each dimension are distinct, $\hat{F}^{M\times N}$ having K harmonics can be represented as follows,

$$\hat{F}^{M\times N} = PCQ^T,$$

where P, Q are Vandermonde structured matrices and $C = diag\{c_1, \cdots, c_k\}$ is a diagonal matrix. Specifically, P, Q are defined:

$$P^{M\times K} = \begin{bmatrix} 1 & 1 & \cdots & 1 \\ p_1 & p_2 & \cdots & p_K \\ \vdots & \vdots & \ddots & \vdots \\ p_1^{M-1} & p_2^{M-1} & \cdots & p_K^{M-1} \end{bmatrix}, \quad Q^{N\times K} = \begin{bmatrix} 1 & 1 & \cdots & 1 \\ q_1 & q_2 & \cdots & q_K \\ \vdots & \vdots & \ddots & \vdots \\ q_1^{N-1} & q_2^{N-1} & \cdots & q_K^{N-1} \end{bmatrix}.$$

For example, in our localization microscopy case, harmonic pair (P_k, Q_k) corresponds to $(e^{-j2\pi\frac{x_k}{M}}, e^{-j2\pi\frac{y_k}{N}})$ and c_k is an intensity of k-th signal at (x_k, y_k). Vandermonde structure is the most important property, used in this harmonic retrieval. In order to utilize Vandermonde structure, four sub-matrices $F_{tl}, F_{tr}, F_{bl}, F_{br}$ are constructed by omitting out-most column and row of $\hat{F}$:

$$\hat{F}_{tl} = \underline{\hat{F}}|\ , \quad \hat{F}_{tr} = \underline{\hat{F}}\ , \quad \hat{F}_{bl} = \overline{\hat{F}}|\ , \quad \hat{F}_{br} = |\overline{\hat{F}}.$$

For example, $\hat{F}_{tl}^{(M-1)\times(N-1)}$ is a top-left sub-matrix of $\hat{F}^{M\times N}$. Then, ACMP algorithm constructs two type of matrix pencils which are written as follows,

$$\textbf{Horizontal}: \quad \hat{F}_{tr} - \alpha\hat{F}_{tl} = \underline{P}C(W_p - \alpha I)\underline{Q}^T, \quad \hat{F}_{br} - \alpha\hat{F}_{bl} = \overline{P}C(W_P - \alpha I)\underline{Q}^T,$$

$$\textbf{Vertical}: \quad \hat{F}_{br} - \beta\hat{F}_{tr} = \underline{P}C(W_Q - \beta I)\overline{Q}^T, \quad \hat{F}_{bl} - \beta F_{tl} = \underline{P}C(W_Q - \beta I)\underline{Q}^T,$$

$$W_P^{K\times K} = diag\{p_1, p_2, \cdots, p_K\}, \quad W_Q^{K\times K} = diag\{q_1, q_2, \cdots, q_K\}.$$

All these matrix pencils have full rank except α or β is equal to the one of harmonics p_k or q_k, respectively. Based on this fact, ACMP can recover diagonal matrices W_P and W_Q whose diagonal components correspond to p_k and q_k, respectively.

Basic ACMP Algorithm Summary

1. compute SVD of F_{tl}

$$F_{tl} = U \cdot \Sigma \cdot V^H$$

2. multiply two type of matrix pencils on the left by U^H and on the right by V

$$\begin{aligned} U^H (F_{tr} - \alpha F_{tl}) V &= C_{tr} - \Sigma \\ U^H (F_{bl} - \alpha F_{tl}) V &= C_{bl} - \Sigma \end{aligned}$$

3. compute eigenvalue decomposition of

$$\Sigma^{-1} C_{tr} = G^{-1} W_P G$$

4. apply eigentransformations G to

$$G \left(\Sigma^{-1} C_{bl}\right) G^{-1} = W_Q$$

4. EXPERIMENTAL RESULTS

We analysed the performance of the proposed algorithm using both numerical experiments and real live-cell PALM imaging.

4.1 Numerical experiments

First, we validated our parametric PSF estimation method. For the analysis, high-density image patches were generated under various signal to noise ratio (SNR). Since signal power is mostly concentrated in a low-frequency band while noise power is widely distributed, Fourier coefficients only from a low-frequency band are used to construct a Hankel matrix $\mathscr{H}\{\frac{\hat{G}[\boldsymbol{\omega}]}{\hat{H}_\sigma[\boldsymbol{\omega},]}\}$. Based on Eq. (10), we plotted the values of Schatten norm ($p = 0.6$) of $\|\mathscr{H}\{\frac{\hat{G}[\boldsymbol{\omega}]}{\hat{H}_\sigma[\boldsymbol{\omega},]}\}\|_p$ along various PSF widths in terms of the parameter σ. This is repeated 30 times for every SNR. As shown in Fig 2., the minimum value of the Schatten norm is close enough to the true value. This tells us that the method can provide reliable estimation results.

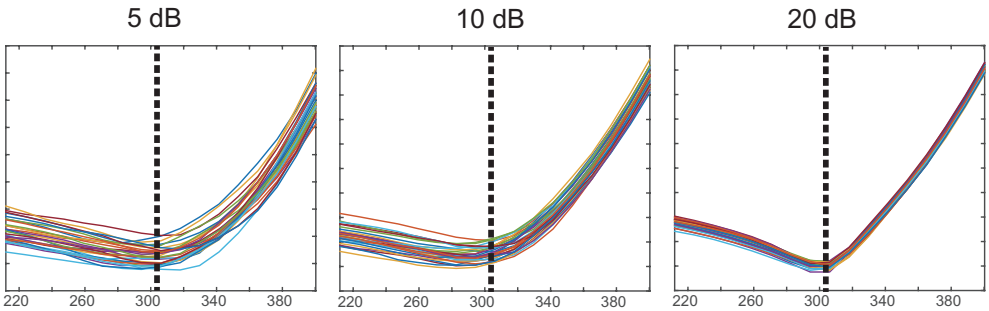

Figure 2. Performance analysis of PSF estimation: values of Schatten norm ($p = 0.6$) of $\|(\mathscr{H}\{\frac{\hat{G}[\boldsymbol{\omega}]}{\hat{H}_\sigma[\boldsymbol{\omega},]}\}\|_p$ are plotted along various widths σ. The dotted black line denotes the true width.

We also evaluated general localization performances of the proposed algorithm in comparison to our previous algorithm FALCON over wide imaging densities. For this simulation study, two set of simulated images were generated under realistic low SNR live imaging conditions of localization microscopy. Specifically, the two photon-emission rates (or signal intensity statistics) of molecule are (300,150) and (150,50) in terns of (mean, standard deviation). Performance analysis was performed by matching each localized one with the closest true molecule within 150 nm range, and then measuring 3 performance scores:[15] recall rate ($\frac{A \cap B}{B}$), Jaccard index ($\frac{A \cap B}{A \cup B}$), localization error (root mean squared). Here, A is the number of localizations, B is total number of true

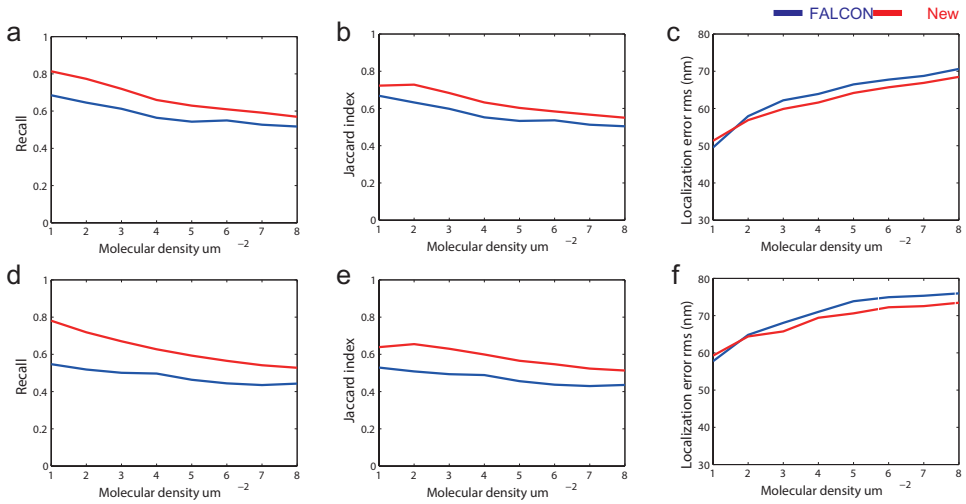

Figure 3. Localization performances of the proposed method in comparison with FALCON along wide range of imaging densities. The simulated images were generated with random distribution of molecules. (a,d) recall rate, (b,e) Jaccard index, (c,f) localization error (r.m.s). (a-c) corresponding to photon-emission (300,150) and (d-f) corresponding to photon-emission (150,50)

molecules. The proposed algorithm shows distinct improvements in recall rate and Jaccard index as shown in Fig. 3., inferring that it localizes more molecules with lower false positive localizations. In the lower SNR case, the improvement is even more distinct.

4.2 Live cell experiments

Finally, the algorithm was experimentally demonstrated with live mitochondria cells on division. We labelled fluorescence probes ("Mitotracker") to the inter-membrane space of the mitochondria, which results in block matrix structure, called cristae. Mitochondria are extremely light-sensitive organelles. Typical irrandiances (10 kW/cm^2) used for localization microscopy lead to sparse photoswitching and high photon yields per molecule, which ultimately results in high spatial resolution. Applying these conditions to the mitochondria over extended periods of time (as short as 60 s) would cause blebbing and almost immediately freeze their motility: this of course, leads to mitochondrial death and perturbs biologically interesting processes. Thus, it is necessary to apply lower irradiances, which leads to lower SNR and higher density dataset. The new method and FALCON algorithm were used to reconstruct the dataset. In fig. 4., the proposed method shows improvement of a spatial resolution as compared to FALCON, preserving clearer cristae structure.

5. CONCLUSION

In this paper, we introduced the new localization algorithm using annihilating filter-based low rank Hankel structured matrix approach. According to ALOHA principle, sparsity property in image space directly infer that a low-rank Hankel matrix can be constructed from its Fourier spectrum. This duality allows the new algorithm to perform data-adaptive PSF estimation, deconvolution, and grid-free localization all in Fourier domain. The method not only can be working as stand-alone without any training dataset for PSF estimation, but also provides truly continuously localization results, which overcomes the limitations of our previous algorithm. Moreover, the method is computationally efficient because all optimizations are conducted in Fourier domain only. The efficacy of the proposed method have been well demonstrated in numerical and experimental study both. These experiments confirmed that the proposed method is more robust to low-SNR and high-density data. Thus, it enables super-resolution imaging with the faster temporal resolution.

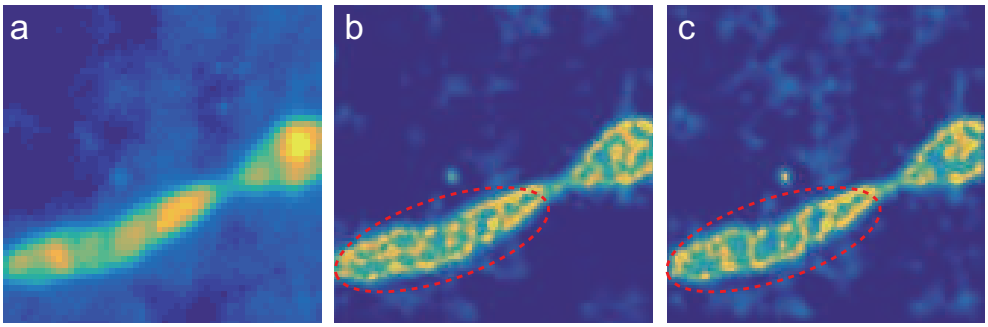

Figure 4. Experimental results of live mitochondria imaging. An wide-field image (a) constructed from 300 raw frames. Super-resolution images reconstructed by FALCON (b) and the proposed method (c). The proposed method preserves the matrix-like structure of cristae, denoted in red circle.

REFERENCES

[1] Min, J., Vonesch, C., Kirshner, H., Carlini, L., Olivier, N., Holden, S., Manley, S., Ye, J. C., and Unser, M., "FALCON: fast and unbiased reconstruction of high-density super-resolution microscopy data," *Sci. Rep.* **4** (2014).

[2] Min, J., Holden, S. J., Carlini, L., Unser, M., Manley, S., and Ye, J. C., "3d high-density localization microscopy using hybrid astigmatic/biplane imaging and sparse image reconstruction," *Biomedical Optics Express* **5**(11), 3935–3948 (2014).

[3] Rust, M. J., Bates, M., and Zhuang, X., "Sub-diffraction-limit imaging by stochastic optical reconstruction microscopy STORM," *Nat. Methods* **3**(10), 793–796 (2006).

[4] Hess, S. T., Girirajan, T. P., and Mason, M. D., "Ultra-high resolution imaging by fluorescence photoactivation localization microscopy," *Biophys. J.* **91**(11), 4258 (2006).

[5] Betzig, E., Patterson, G. H., Sougrat, R., Lindwasser, O. W., Olenych, S., Bonifacino, J. S., Davidson, M. W., Lippincott-Schwartz, J., and Hess, H. F., "Imaging intracellular fluorescent proteins at nanometer resolution," *Science* **313**(5793), 1642–1645 (2006).

[6] Holden., S. J., Uphoff., S., and Kapanidis, A. N., "DAOSTORM: an algorithm for high-density super-resolution microscopy," *Nat. Methods* **8**(4), 279–280 (2011).

[7] Huang, F., Schwartz, S. L., Byars, J. M., and Lidke, K. A., "Simultaneous multiple-emitter fitting for single molecule super-resolution imaging," *Biomed. Opt. Express* **2**(5), 1377–1393 (2011).

[8] Zhu, L., Zhang, W., Elnatan, D., and Huang, B., "Faster storm using compressed sensing," *Nat. Methods* **9**(7), 721–723 (2012).

[9] Jin, K. H., Lee, D., and Ye, J. C., "A general framework for compressed sensing and parallel mri using annihilating filter based low-rank hankel matrix," *arXiv preprint arXiv:1504.00532* (2015).

[10] Jin, K. H. and Ye, J. C., "Annihilating filter based low rank hankel matrix approach for image inpainting," *Image Processing, IEEE Transactions on* **24**(11), 3498–3511 (2015).

[11] Hua, Y., "Estimating two-dimensional frequencies by matrix enhancement and matrix pencil," *Signal Processing, IEEE Transactions on* **40**(9), 2267–2280 (1992).

[12] Vanpoucke, F., Moonen, M., and Berthoumieu, Y., "An efficient subspace algorithm for 2-d harmonic retrieval," in [*Acoustics, Speech, and Signal Processing, 1994. ICASSP-94., 1994 IEEE International Conference on*], **4**, IV–461, IEEE (1994).

[13] Afonso, M. V., Bioucas-Dias, J. M., and Figueiredo, M. A., "Fast image recovery using variable splitting and constrained optimization," *IEEE Trans. Image Process* **19**(9), 2345–2356 (2010).

[14] Halko, N., Martinsson, P.-G., and Tropp, J. A., "Finding structure with randomness: Probabilistic algorithms for constructing approximate matrix decompositions," *SIAM review* **53**(2), 217–288 (2011).

[15] Sage, D., Kirshner, H., Pengo, T., Stuurman, N., Min, J., Manley, S., and Unser, M., "Quantitative evaluation of software packages for single-molecule localization microscopy," *Nature methods* (2015).